

Supplement to

Waveguide-based platform for large-FOV imaging of optically-active defects in 2D materials

Evgenii Glushkov¹, Anna Archetti², Anton Stroganov^{1,2*}, Jean Comtet¹, Mukeshchand Thakur¹, Vytautas Navikas¹, Martina Lihter¹, Juan Francisco Gonzalez Marin³, Vitaliy Babenko⁴, Stephan Hofmann⁴, Suliana Manley², Aleksandra Radenovic¹

¹ Laboratory of Nanoscale Biology, Institute of Bioengineering,

² Laboratory of Experimental Biophysics, Institute of Physics, and

³ Laboratory of Nanoscale Electronics and Structures, Institute of Electrical Engineering and Institute of Material Science,

École Polytechnique Fédérale de Lausanne (EPFL), 1015 Lausanne, Switzerland

⁴ Department of Engineering, University of Cambridge, JJ Thomson Avenue, CB3 0FA Cambridge, United Kingdom

* current address: LIGENTEC, SA

Corresponding authors: evgenii.glushkov@epfl.ch and aleksandra.radenovic@epfl.ch

Table of Contents

Supplementary Figures	S3
Figure S1 Schematic representation of the typical process flow	S3
Figure S2 Adding lensed fibers to an existing microscope	S4
Figure S3 Large-area CVD-grown MoS ₂ flakes transferred to the waveguide chips	S5
Figure S4 hBN flakes transferred to different imaging wells on different waveguides	S6
Figure S5 Spectra of optically-active defects in hBN, transferred onto the waveguide chips	S7
Figure S6 Temporal properties of the blinking emitters in hBN	S8
Figure S7 Estimating average densities of optically-active defects in hBN flakes.....	S9
Bibliography	S10

Supplementary Figures

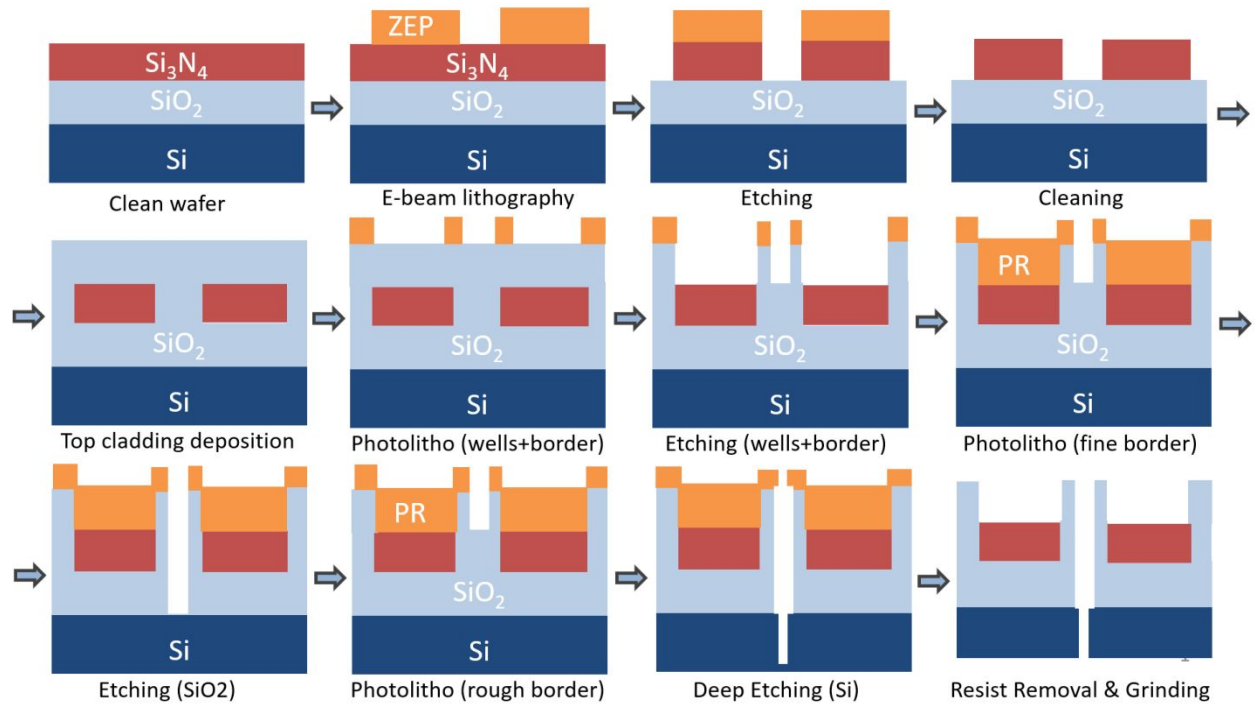


Figure S1 Schematic representation of the typical process flow used to fabricate the waveguide chips. The detailed description of the fabrication steps and the parameters used is given in Ref. 1.

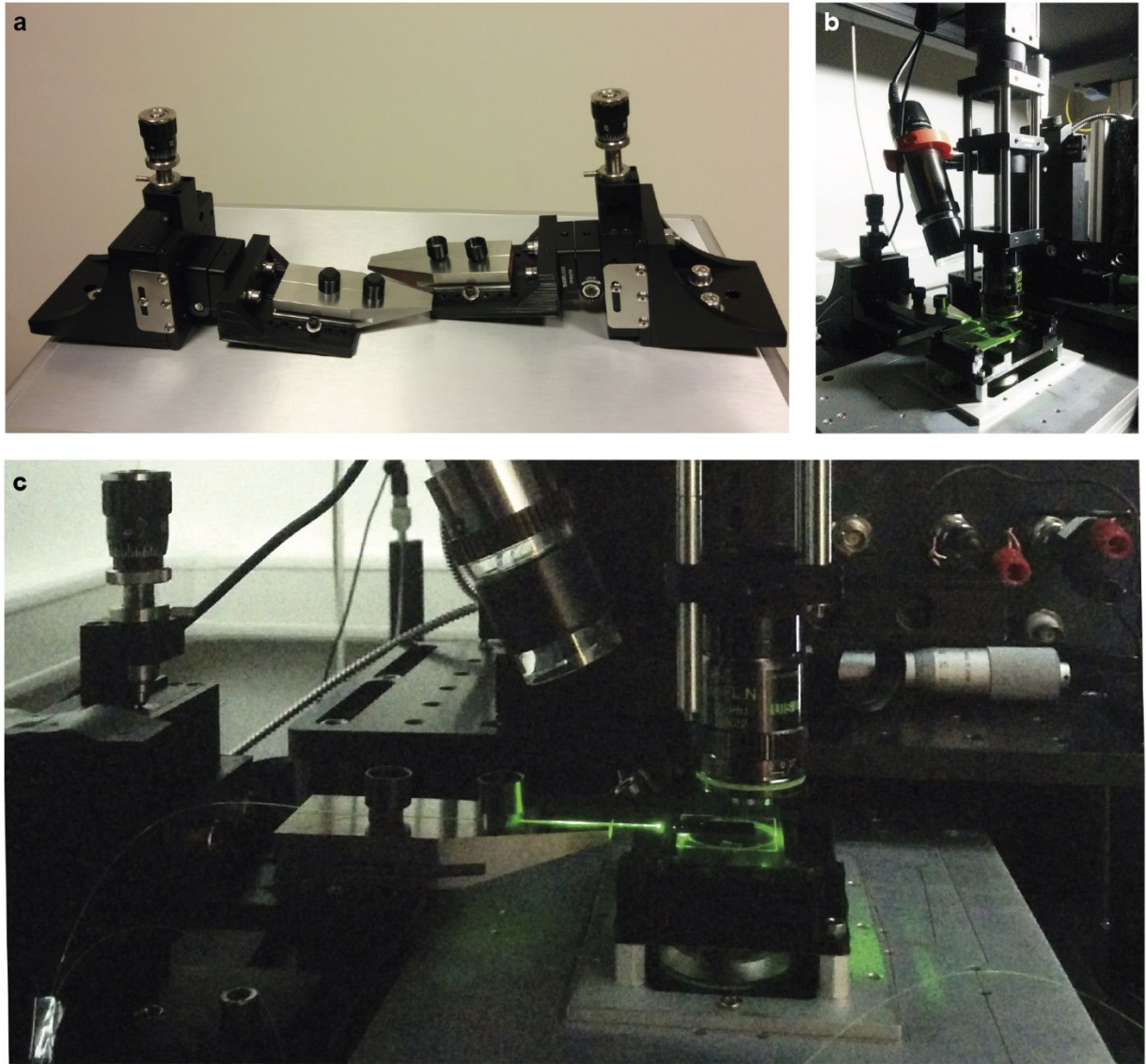


Figure S2 Adding lensed fibers to an existing microscope to couple light inside the waveguide chip. (a) Custom-made holders for lensed fibers, consisting of standard components (Thorlabs, 1xPT1 translation stages for each axis with AP90 right-angle plate or 1xPT3A assembly, and HFV002 fiber holder) and a 3D-printed adapter (STL file available at: doi.org/10.5281/zenodo.3354120). The optional adjustable flip platform (Thorlabs, FP90) can be added to couple light into the on-chip grating couplers at a certain angle. The lensed fiber itself can be purchased from OZ Optics, item number TSMJ-3A-633-5/125-0.25-10-2.5-12-1. (b) The optical setup (inverted microscope) with an added lensed fiber on the custom-made holder. The green laser is coupled into the on-chip waveguide by aligning the lensed fiber tip with the entrance of the waveguide. The USB-microscope (DinoLite) and a small CMOS camera (Thorlabs) on top are used for alignment. (c) A zoom-in, showing the coupled laser light inside the lensed fiber and the

waveguide chip.

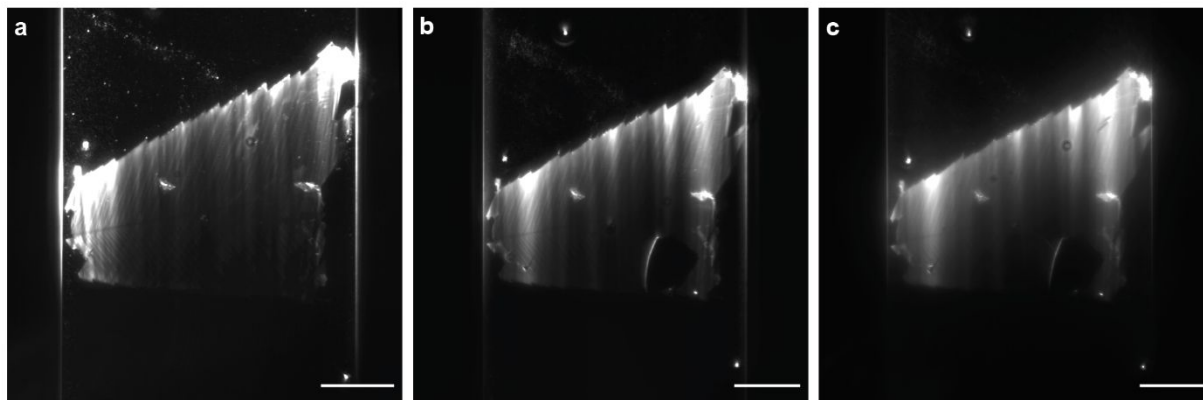


Figure S3 Large-area CVD-grown MoS₂ flakes transferred to the waveguide chips. (a) Imaged in air using an air objective (Olympus LMPlanFL N, 100x, NA 0.8) (b, c) The same flake imaged using a dipping objective (Nikon CFI Plan 100XC W, 100x, NA 1.1) in DI water and in 70% ethanol, respectively. The blur in c) comes from the index mismatch between water and ethanol. Scale bar: 25 μm

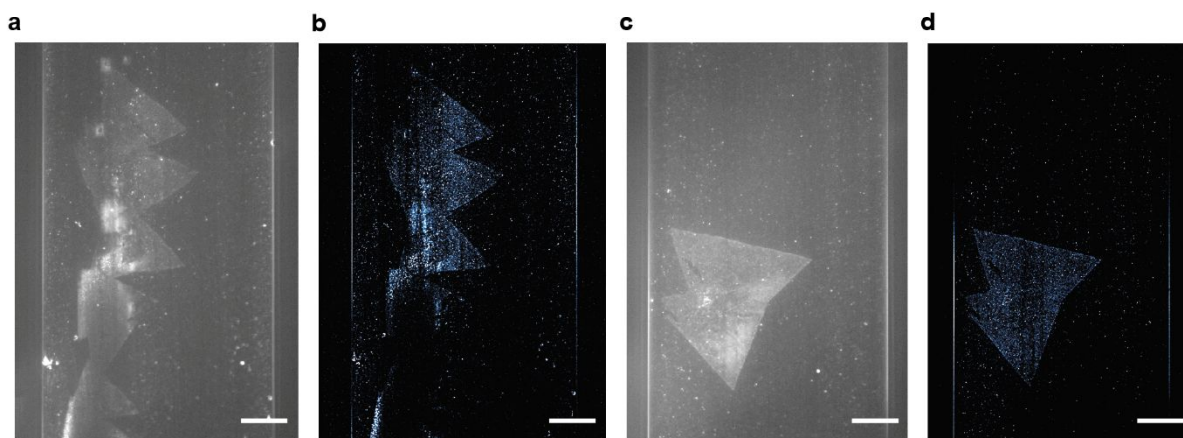


Figure S4 hBN flakes transferred to different imaging wells on different waveguides. (a, c) Fluorescent images obtained using 641 nm laser excitation (5'000 frames, averaged). (b, d) Reconstructed super-resolved images, obtained from the same stack of 2'000 frames. Scale bar 20 μm .

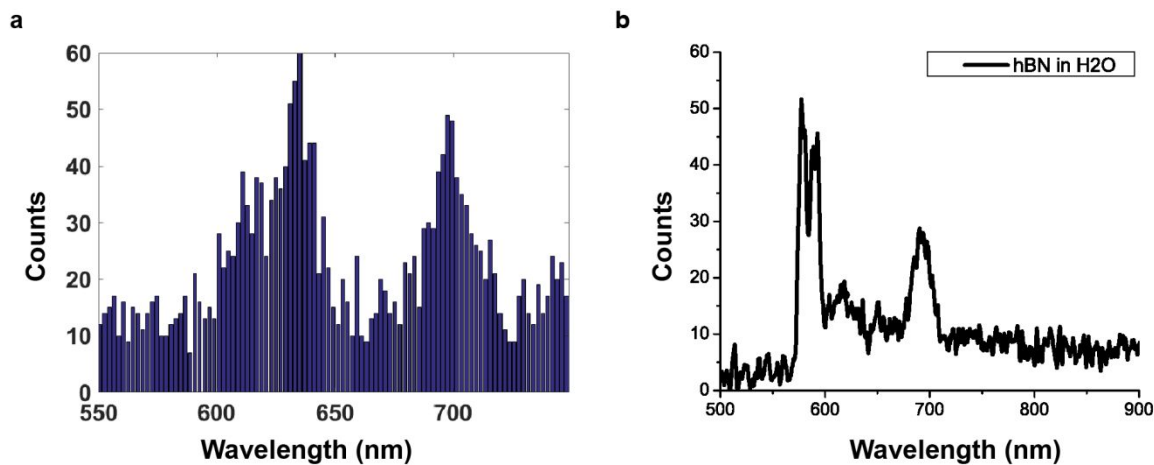


Figure S5 Spectra of optically-active defects in hBN, transferred onto the waveguide chips. (a) Spectrum of an ensemble of emitters in hBN, obtained using a widefield spectral super-resolution technique from Ref. 2, averaged over a field of view of $25 \times 25 \mu\text{m}^2$. (b) Spectrum of emitters in hBN collected from a diffraction-limited spot using a fibre-coupled spectrometer (QE Pro, Ocean Optics) with the following parameters: $200 \mu\text{W}$ excitation power, 1s acquisition time, 100 averages. Both spectra were obtained using 561 nm laser excitation and are in good agreement with the published data from Ref. 2 (Type B emitters). The differences in the two spectra are due to different dichroic mirrors on the two setups used.

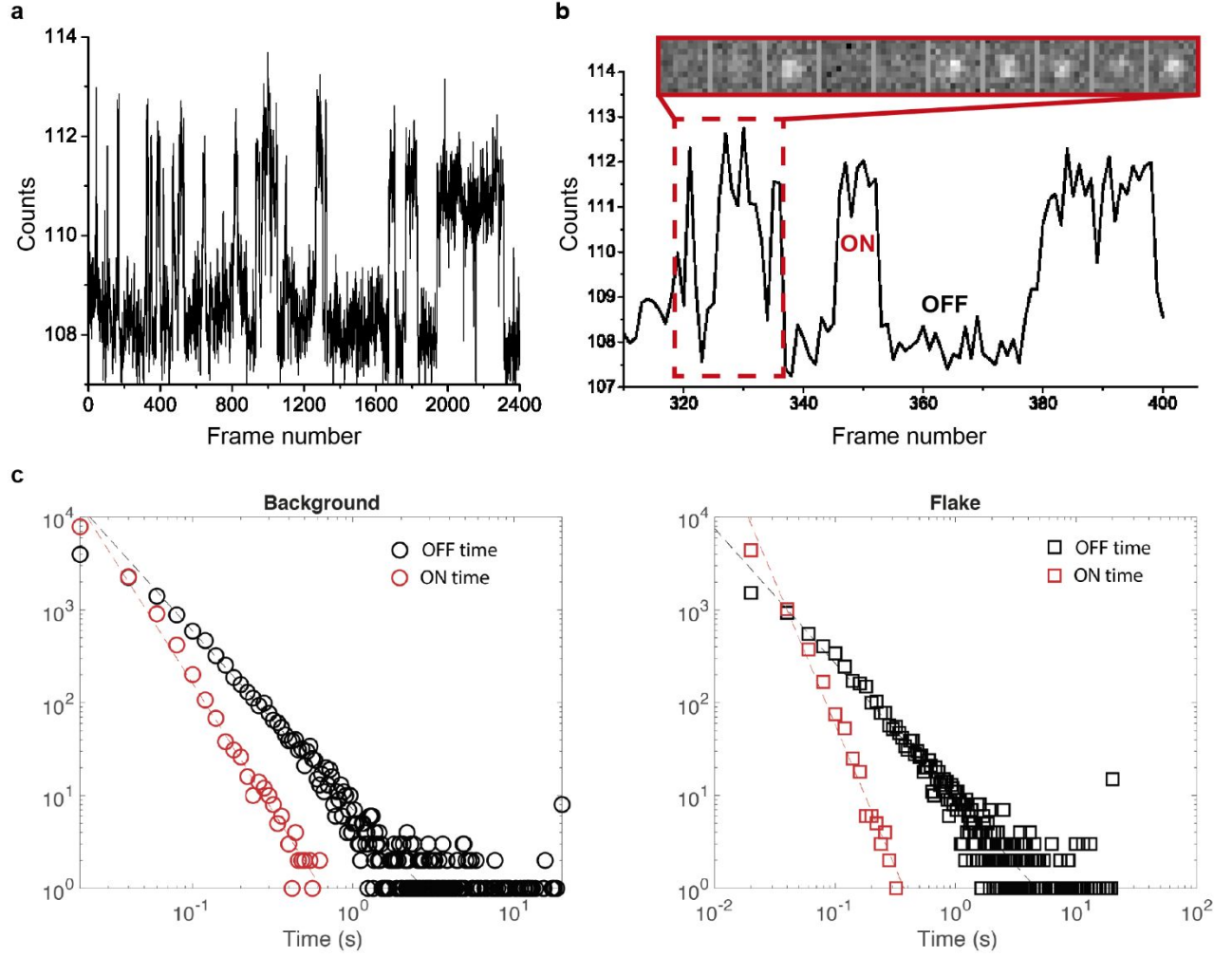


Figure S6 Temporal properties of the blinking emitters in hBN (a) A typical timetrace of a single emitter from Fig. 3c, showing mean counts over the acquired image stack. (b) A zoom into a region from (a) showing distinct ON and OFF states for the emitter, depicted in the frame series above. (c) Blinking statistics of the hBN emitters on waveguides (and the parasitic background defects in the silica cladding). The distribution of ON and OFF times has a power law dependence with the following values: $\alpha_{\text{ON}} = -2.7$, $\alpha_{\text{OFF}} = -1.9$ (background); $\alpha_{\text{ON}} = -3.0$, $\alpha_{\text{OFF}} = -1.45$ (hBN). The values of ON and OFF times for the CVD-grown hBN flakes are consistent with the previously published data³ on the same material, though the exact values might be affected by the substrate.

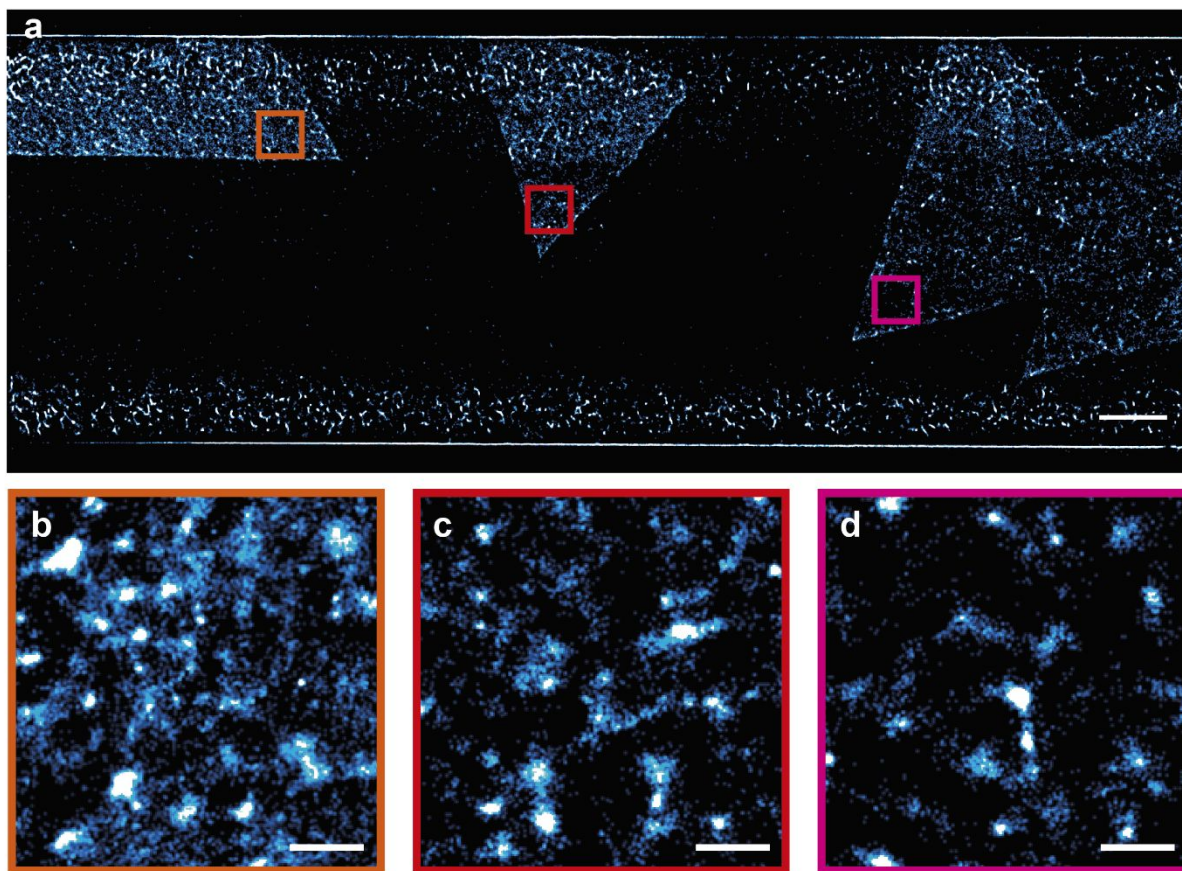


Figure S7 Estimating average densities of optically-active defects in hBN flakes. a) Reconstructed super-resolved image from Fig. 3c. The colored squares show the ROIs on three different hBN flakes chosen to estimate the average densities of defects. (b-d) Corresponding zoom-ins into ROIs from (a). The average densities are: $341 \mu\text{m}^{-2}$ (b), $234 \mu\text{m}^{-2}$ (c) and $116 \mu\text{m}^{-2}$ (d), and were calculated as the number of emitters per square micrometer using the data generated during the localization process⁴. To calculate the number of emitters, all localizations were merged using the ThunderSTORM⁵ merge function with the following parameters: maximum distance – 20nm, max. frames per molecule – 0 (unlimited), maximum off frames -500. The manual selection of ROIs can be replaced by an image recognition algorithm, segmenting the hBN flakes from the background and calculating the number of emitters in each area (e.g. using the free ilastik⁶ software). Scale bar: 10 μm (a), 1 μm (b-d)

Bibliography

1. Archetti, A. *et al.* Waveguide-PAINT offers an open platform for large field-of-view super-resolution imaging. *Nat. Commun.* **10**, 1–9 (2019).
2. Comtet, J. *et al.* Wide-Field Spectral Super-Resolution Mapping of Optically Active Defects in Hexagonal Boron Nitride. *Nano Lett.* **19**, 2516–2523 (2019).
3. Stern, H. L. *et al.* Spectrally Resolved Photodynamics of Individual Emitters in Large-Area Monolayers of Hexagonal Boron Nitride. *ACS Nano* **13**, 4538–4547 (2019).
4. Feng, J. *et al.* Imaging of optically active defects with nanometer resolution. *Nano Lett.* **18**, 1739–1744 (2018).
5. Ovesný, M., Křížek, P., Borkovec, J., Švindrych, Z. & Hagen, G. M. ThunderSTORM: a comprehensive ImageJ plug-in for PALM and STORM data analysis and super-resolution imaging. *Bioinformatics* **30**, 2389–2390 (2014).
6. Berg, S. *et al.* ilastik: interactive machine learning for (bio)image analysis. *Nat. Methods* (2019). doi:10.1038/s41592-019-0582-9